Experimental Validation of a Coupled Solid- and Gas-Phase Model for Combustion and Gasification of Wood Logs

Antonio Galgano,[†] Colomba Di Blasi,*,[†] Andrej Horvat,[‡] and Yehuda Sinai[‡]

*Dipartimento di Ingegneria Chimica, Università degli Studi di Napoli "Federico II",
P.le V. Tecchio, 80125 Napoli, Italy, and ANSYS Europe Ltd., West Central 127, Milton Park,
Abingdon OX14 4SA, United Kingdom*

A solid−gas-phase model for thick wood gasification/combustion is extensively studied, after a re-examination of the kinetic constants for the char gasification reactions. The solid-phase model, which includes the description of all the relevant heat and mass transfer phenomena and chemical reactions, is coupled with a CFD code for the gas-phase processes. Both the gasification and combustion of single wood logs are simulated (log radius in the range of 0.06−0.1 m, initial moisture content, on a dry basis, 1−81%, inlet gas temperature 1253−1613 K, inlet gas velocity 0.5−1.0 m/s, and various compositions of the gaseous mixture). For comparison purposes, a solid-phase model, with global heat and mass transfer coefficients and a constant-property gas phase, is also considered. Although both models predict the mass loss dynamics to be qualitatively similar, the solid-phase model overestimates the total heat flux and underestimates the char combustion rate. Extensive experimental validation of both models is carried out in terms of conversion time and average mass-loss rates. Acceptable agreement is obtained for the comprehensive model, whereas in the other case, the conversion times are generally underestimated and the average mass loss rates are overestimated. However, improvements in the predictive capabilities of the solid-phase model could be achieved through the introduction of corrective factors for the external heat and mass transfer coefficients.

1. Introduction

Models of wood log or particle gasification and combustion are of interest in the sectors of heat and power production from biomass and forest fire development and propagation. It has been pointed out that whole-tree-sized feed has several advantages over wood chips for industrial market fuels.[1−3] They consist of reduced energy requirements for feed preparation, more favorable transportation and storage, and easier drying of the stored material. In addition, for grate furnaces, whole-tree-sized fuel is characterized by higher conversion degrees and reduced costs of gas cleaning devices, as a consequence of the fewer particles formed and entrained by the gas stream. Environmentally, the smoldering of wood logs, after forest fires, is important as a source of pollutants, biomass consumption, and for the possible initiation of new fires.[4] Again, in this case, compared to biomass boilers, the size of the burning specimen is usually larger.

A significant number of kinetic and transport models is available for the first step of wood conversion (i.e., pyrolysis), as discussed in a review by Di Blasi.[5] On the other hand, only few models take into account the heterogeneous processes of gasification and combustion. In the simplest cases, wood/biomass devolatilization and char conversion are considered as two separate and sequential processes. Examples are the models by Mukunda et al.,[6] Saastamoinen and Richard,[7] Winter et al.,[8] Leckner et al.,[9] and Gera et al.[10] Transport models for the sole processes related to char conversion are presented in some papers.[11−13] In other cases, for biomass samples[1−4,14] or black liquor drops,[15,16] the simultaneous presence of both pyrolysis and combustion/gasification reactions is considered. In all cases,

(1) Ragland, K. W.; Boerger, J. C.; Baker, A. J. *For. Prod. J.* **1988**, *38*, 27−32.

(2) Bryden, K. M.; Ragland, K. W. *Energy Fuels* **1996**, *10*, 269−275.

(3) Bryden, K. M.; Ragland, K. W. In *Developments in Thermochemical Biomass Conversion*; Bridgwater, A. V., Boocock, D. G. B., Eds.; Blackie A & P: London, 1997; pp 1331−1345.

(4) de Souza Costa, F.; Sandberg, D. *Combust. Flame* **2004**, *139*, 227−238.

(5) Di Blasi, C. In *Fast Pyrolysis of Biomass: A Handbook*; Bridgwater, A. V., Ed.; CPL Press: Newbury, 2005; pp 121−146.
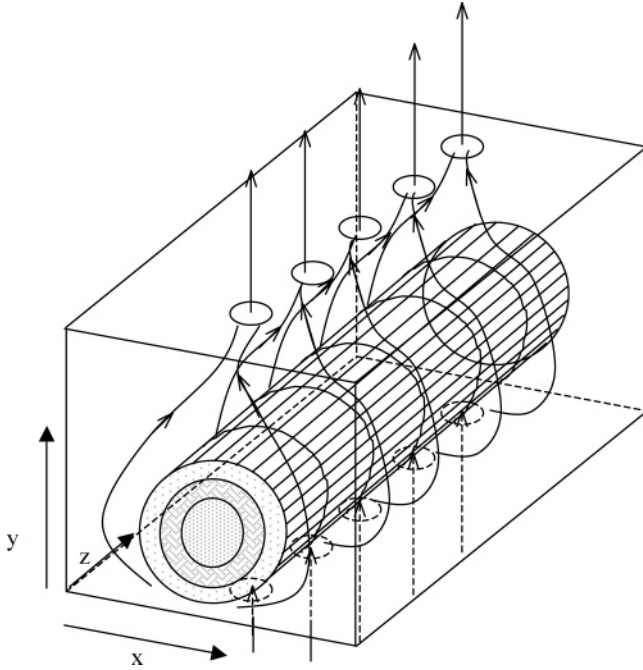
(6) Mukunda, H. S.; Paul. P. J.; Shrinivasa, U.; Rajan, N. K. S. *Proceedings of the 20th International Symposium on Combustion*; The Combustion Institute: Pittsburgh, 1984; pp 1619−1628.

(7) Saastamoinen, J.; Richard, J. In *Research in Thermochemical Biomass Conversion*; Bridgewater, A. V., Kuester, J. L., Eds.; Elsevier: London, 1985; pp 221−235.

(8) Winter, F.; Prah, M. E.; Hofbauer, H. *Combust. Flame* **1997**, *108*, 302−314.

(9) Leckner, B.; Hansson, K. M.; Tullin, C.; Borodulya, A. V.; Dikalenko, V. A.; Palchonok, G. I. *Proceedings of the 15th International Conference on Fluidized Bed Combustion*; American Society of Mechanical Engineers: New York, 1999; pp 1−14.

(10) Gera, D.; Mathur, M. P.; Freeman, M. P.; Robinson, A. *Energy Fuels* **2002**, *16*, 1523−1532.

(11) Dasappa, S.; Paul, P. J.; Mukunda, H. S.; Shrinivasa, U. *Chem. Eng. Sci.* **1994**, *49*, 223−32.

(12) Dasappa, S.; Sridhar, H. V.; Paul, P. J.; Mukunda, H. S.; Shrinivasa, U. *Proceedings of the 25th International Symposium on Combustion*; The Combustion Institute: Pittsburgh, 1994; pp 1619−1628.

(13) Dasappa, S.; Paul, P. J.; Mukunda, H. S.; Shrinivasa, U. *Proceedings of the 27th Symposium (International) on Combustion*; The Combustion Institute: Pittsburgh, 1998; pp 1335−1342.

(14) Ouedraogo, A.; Mulligan, J. C.; Cleland, J. G. *Combust. Flame* **1988**, *114*, 1−12.

(15) Jarvinen, M.; Zevenhoven, R.; Vakkilainen, E. *Combust. Flame* **2002**, *131*, 357−70.

(16) Jarvinen, M.; Zevenhoven, R.; Vakkilainen, E.; Forssen, M. *Biomass Bioenergy* **2003**, *24*, 495−509.

Figure 1. Schematic of the experimental system used by Bryden and Ragland[3] for the gasification/combustion of single wood logs.

even though gas-phase processes influence the solid-phase dynamics and play a crucial role for the transition from smoldering to flaming combustion, they are usually disregarded or subjected to highly simplified treatments (for instance, see Mukunda et al.[6]).

An exception is the model recently developed by Galgano and Di Blasi.[17] For the solid-phase processes, the model is based on the unreacted-shrinking-core treatment, specifically developed for the gasification/combustion of thick wood samples. The simultaneous occurrence of drying, pyrolysis, and char gasification/oxidation is taken into account with the description of the most important transport phenomena. The solid-phase model is coupled with a CFD model for the gas-phase processes. Coupling between the two models at the solid/gas interface is made by assuming that the characteristic times of the gas-phase processes are much shorter than those of the solid phase. However, model simulation and analysis is limited to a single test case. The primary objectives of this study are concerned with the experimental validation of the previously developed comprehensive model to better understand the role played by simplifications usually introduced in the description of the gas-phase processes. Moreover, in connection to the above analyses, a re-examination of the global kinetics of wood-char gasification is presented.

2. Mathematical Modeling

2.1. Solid- and Gas-Phase Model. The gasification/combustion of single wood logs is simulated as in the experimental system by Bryden and Ragland.[3] The system (Figure 1) consists of a furnace with a 1.5 m long, 0.305 m wide, and 0.368 m high working chamber, where a wood log is exposed to a hot gas flow with variable concentrations of O_2, CO_2, CO, and H_2O. The gas enters the furnace through five holes on the bottom surface. After it mixed with the volatiles generated from wood conversion and occurrence of homogeneous reactions, the gaseous stream exits through five holes on the upper surface. The mathematical model of the problem

(17) Galgano, A.; Di Blasi, C. *Prog. Comput. Fluid Dyn.* **2006**, 6, 287–302.

Table 1. Mass and Enthalpy Balances for the Gasification/Combustion of Wood in the Presence of the Evaporation, Pyrolysis, and Gasification/Combustion Fronts

char layer ($R_p \leq r \leq R_e$)

$$\frac{1}{r}\frac{d}{dr}(rm_v) = 0, \quad S_p M_v|_{R_p^+} = m_u + m_p \quad \text{(1a, 1b)}$$

$$0 = \frac{1}{r}\frac{\partial}{\partial r}[rm_v c_g T] + \frac{1}{r}\frac{\partial}{\partial r}\left[k_c^* r \frac{\partial T}{\partial r}\right] \quad \text{(2)}$$

$$S_c k_c^* \frac{\partial}{\partial r}\big|_{r=R_0} = S_c q_s - \sum_{i=a1}^{a3} -\Delta h_i \varpi_i, \quad T|_{R_p^+} = T|_{R_p^-} \quad \text{(3a, 3b)}$$

$$S_c F_j + x_{0,j} m_p + \delta_{H_2O,j} m_p - x_{s,j}(m_u + m_p + \sum_{i=a1}^{a3} \varpi_i) = \sum_{i=a1}^{a3}\sum_j s_{i,j}\frac{M_j}{M_C}\varpi_i \quad \text{(4)}$$

$j = CH_4, CO, CO_2, H_2, H_2O, O_2; \delta_{H_2O,j} = 1$ for $j = H_2O$, $\delta_{H_2O,j} = 0$ for $j \neq H_2O$

$$y_{s,j} = \frac{M_s}{M_j}x_{s_j} \quad \text{(5)}$$

$$S_c \rho_c \frac{dR_c}{dt} = -\sum_{i=a1}^{a3}\varpi_i, \quad R_e(0) = R_0 \quad \text{(6a, 6b)}$$

dry wood layer ($R_u \leq r \leq R_p$)

$$\omega_p = A_p \exp(-E_p/\mathscr{R}T)S_p \nu_w \quad \text{(7)}$$

$$\frac{dR_c}{dt} = -A_p \exp\left(-\frac{E_p}{\mathscr{R}T}\right), \quad R_p(0) = R_0 \quad \text{(8a, 8b)}$$

$$m_p = \nu_v \omega_p \quad \text{(9)}$$

$$\nu_w c_w \frac{\partial T}{\partial r} = \frac{1}{r}\frac{\partial}{\partial r}[rm_v c_u T] + \frac{1}{r}\frac{\partial}{\partial r}\left[k_w^* r \frac{\partial T}{\partial r}\right] \quad \text{(10)}$$

$$S_p q_c = S_p q_w + m_p \Delta h \ (r = R_p), \quad T|_{R_u} = T_b \ (r = R_u) \quad \text{(11a, 11b)}$$

$$q_c = k_c^* \frac{\partial}{\partial r}|_{R_p^+}, \quad q_w = k_w^* \frac{\partial T}{\partial r}|_{R_p^-} \quad \text{(12a, 12b)}$$

$$\frac{1}{r}\frac{d}{dr}(rm_v) = 0, \quad S_u m_v|_{R_p^+} = m_u \quad \text{(1a, 1c)}$$

moist wood layer ($0 \leq r \leq R_u$)

$$S_u q_u = m_u[\tilde{\lambda} + c_l(T_b - T_0)] + \frac{m_u}{U_0}c_w(T_b - T_0) \quad \text{(13)}$$

$$q_u = k_w^* \frac{\partial T}{\partial r}|_{r=R_u} \quad \text{(14)}$$

$$\frac{dR_u}{dt} = -\frac{m_u}{S_u \rho_w U_0}, \quad R_u(0) = R_0 \quad \text{(15a, 15b)}$$

consists of the solid-phase equations (summarized in Table 1) for the simultaneous presence of the evaporation, pyrolysis, and gasification/combustion processes (for symbols, see the Nomenclature section) and the gas-phase equations, as in the CFX user manual.[18] The assumptions are only briefly discussed, as details can be found in Galgano and Di Blasi.[17] The three-dimensional problem is approached as two-dimensional (x, y) according to the scheme shown in Figure 2. The wood log is placed in the middle of the furnace at a fixed distance of 0.01 m from the bottom surface for the entire duration of the test. The bottom surface is assumed to coincide with the gas-flow entrance, while an opening (1.5 m

(18) *CFX 4.4 Solution Manual*; AEA Technology Engineering Services Inc.; Pittsburgh, 1999.
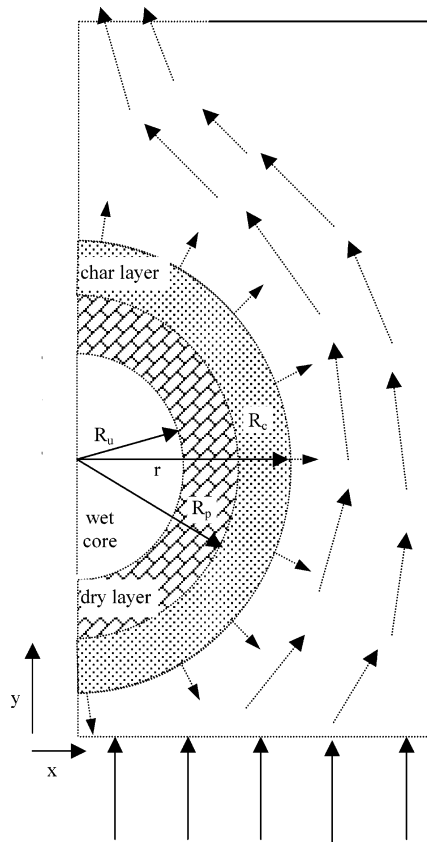
Figure 2. Schematic of the problem (cross-section of the furnace) modeled.

long and 0.05 m wide) situated in the center of the upper surface is assumed to be the exit for the gaseous stream.

A one-dimensional formulation (radial coordinate) is used for the solid-phase processes. Although this assumption may appear to be an oversimplification, a comparison between the one- and two-dimensional models indicates that the average mass-loss rates of the solid and the conversion time are practically unaffected.[17] The coupling between the one-dimensional (solid) and the two-dimensional (gas) description is made using average values of the heat and mass fluxes at the solid/gas interface.

Wood conversion is described according to the unreacted-shrinking-core approximation, discussed in detail by Galgano and Di Blasi[19,20] for the pyrolysis of dry and moist wood. Pyrolysis (a finite-rate one-step reaction) takes place at an infinitely thin surface, separating the char from the dry wood layer. Moisture evaporation also occurs at an infinitely thin, constant-temperature (T_b) front, which separates the moist from the dry region. Experimental validation of the pyrolysis model has been made using the weight-loss characteristics of thick beech wood samples with varied external temperatures and initial moisture contents.[21,22]

Heterogeneous gasification/combustion, described by reactions a1−a3 occurs at the external surface of the char layer, which

$$C + CO_2 \rightleftharpoons 2CO \tag{a1}$$

$$C + H_2O \rightleftharpoons H_2 + CO \tag{a2}$$

$$C + \frac{1}{2}O_2 \rightleftharpoons CO \tag{a3}$$

consists of pure carbon. Although the CO and CO_2 yields from the combustion of char may be functions of the reaction conditions, as in previous studies,[3] it is assumed that only CO is produced. The

rates (kilograms of C per second) of the gasification reactions (a1−a2) are modeled as in Barrio and Hustad[23] and Barrio et al.,[24] respectively

$$\varpi_{a1} = S_c A_{a1} \exp(-E_{a1}/\mathscr{R}T)\rho_c y_{s,CO_2}^{n_{a1}} \tag{16}$$

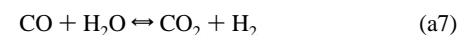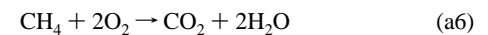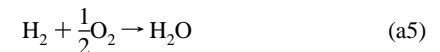$$\varpi_{a2} = S_c A_{a2} \exp(-E_{a2}/\mathscr{R}T)\rho_c y_{s,H_2O}^{n_{a2}} \tag{17}$$

where y_{s,H_2O} and y_{s,CO_2} are the surface mole fractions of H_2O and CO_2. Following previous literature,[1,13,25] the diffusion rate of oxygen to the external surface of the char layer is much slower than the kinetic rate. Thus, the rate of the oxidation reaction (a3) is assumed to be diffusion controlled.

The solid matrix and the gas within the pores are assumed to be in thermal equilibrium, although cracks and fissures in the char layer produce preferential paths for the gas flowing out of the sample. Other assumptions for the stages of drying and pyrolysis are as follows:[19,20] (1) the diffusion of volatile species and water vapor is negligible compared to convection, (2) the pressure is constant, (3) the accumulation of enthalpy and volatile species within the char pores is negligible, (4) the specific heats and the effective thermal conductivities of wood and the pyrolysis products are constant, (5) the char emissivity is equal to 1.0, (6) the moist core of the particle is at ambient (initial) temperature, (7) the heat flux at the drying front is applied exclusively for increasing the surface temperature, from the initial to the evaporation value, and sustaining the endothermic evaporation process, and (8) shrinkage is neglected.

During gasification/combustion, the solid undergoes several stages (initial drying, gasification/combustion of moist wood, gasification/combustion of dry wood, and gasification/combustion of char), which are described by appropriate set of equations, as detailed in Galgano and Di Blasi.[17]

The gas phase, surrounding the wood log, is assumed to be in a steady state:[26−28] the gas-phase characteristic times are typically much shorter than those of the solid-phase processes. Although laminar conditions are considered at the reactor inlet (Re ≈ 800), given that the effects of the thermal degradation of the wood log on the flow field are not known, a $k-\epsilon$ turbulence model modified for low Reynolds number flows is used. To take into account buoyancy effects in the flow, the Boussinesq approximation is implemented.[29]

The O_2, CO, CO_2, H_2, H_2O, CH_4, and N_2 gas species are considered with the following reactions:

$$CO + \frac{1}{2}O_2 \rightarrow CO_2 \tag{a4}$$

$$H_2 + \frac{1}{2}O_2 \rightarrow H_2O \tag{a5}$$

$$CH_4 + 2O_2 \rightarrow CO_2 + 2H_2O \tag{a6}$$

$$CO + H_2O \rightleftharpoons CO_2 + H_2 \tag{a7}$$

(19) Galgano, A.; Di Blasi, C. *Ind. Eng. Chem. Res.* **2003**, *42*, 2101−2111.
(20) Galgano, A.; Di Blasi, C. *Combust. Flame* **2004**, *139*, 16−27.

(21) Di Blasi, C.; Gonzalez Hernandez, E.; Santoro, A. *Ind. Eng. Chem. Res.* **2000**, *39*, 873−82.
(22) Di Blasi, C.; Branca, C.; Santoro, A.; Gonzalez Hernandez, E. *Combust. Flame* **2001**, *124*, 165−77.
(23) Barrio, M.; Hustad, J. E. In *Progress in Thermochemical Biomass Conversion*; Bridgewater, A. V., Ed.; Blackwell Science Ltd.: Oxford, U.K., 2001; pp 47−60.
(24) Barrio, M.; Gobel, B.; Risnes, H.; Henriksen, U.; Hustad, J. E.; Sorensen, L. H. In *Progress in Thermochemical Biomass Conversion*; Bridgewater, A. V., Ed.; Blackwell Science Ltd.: Oxford, U.K., 2001; pp 32−46.
(25) Bruch, C.; Peters, B.; Nussbaumer, T. *Fuel* **2003**, *82*, 729−738.
(26) Di Blasi, C. *Combust. Flame* **1994**, *97*, 225−239.
(27) Di Blasi, C. *Combust. Flame* **1995**, *100*, 332−340.
(28) Di Blasi, C.; Wichman, I. S. *Combust. Flame* **1995**, *102*, 229−240.
(29) Launder, B. E.; Sharma, B. I. *Lett. Heat Mass Transfer* **1974**, *1*, 131−138.

Table 2. Kinetic Constants for the Gas-Phase Reactions

parameter	value	ref
A_{a4}	3.98×10^{17} (m³/mol)$^{0.75}$/s K	2
A_{a5}	10^{11} m³/s mol	2
A_{a6}	9.2×10^6 (m³/mol)$^{0.5}$/s K	2
A_{a7}	2.78 m³/mol s	38
b	0.3 [m^{-1}]	17
A_E	0.0265	39
E_{a4}	166 kJ/mol	2
E_{a5}	42 kJ/mol	2
E_{a6}	80 kJ/mol	2
E_{a7}	12.6 kJ/mol	38
E_E	65.8 kJ/mol	39

The rates of the gas-phase reactions are computed as the minima[30] between the kinetic rates and the turbulence mixing rates by application of the eddy dissipation concept.[31] Thermal radiation is taken into account using the discrete transfer method of Lockwood and Shah.[32]

The one-dimensional solid-phase model and the two-dimensional gas-phase model are coupled at the external shrinking surface of the wood log, where boundary conditions (continuity for temperature, gas species mass fractions, and heat and mass fluxes) are specified.

For comparison purposes, a simplified treatment of the gas-phase processes is also considered, which uses global heat and mass transfer coefficients and conditions coincident with those of the inlet.

2.2. Solution Method. The solution method is described in detail by Galgano and Di Blasi.[17] In summary, the conservation equations for the solid phase are transformed into a set of algebraic and ordinary differential equations, by applying the heat balance integral method.[19,20] Mass, momentum, species, and enthalpy conservation equations for the gas phase are solved with the CFX[18] computational fluid dynamics code. The code is based on the finite volume method for the discretization of the governing equations. The gas-phase equations are solved only for a limited number of solutions of the solid-phase equations. Indeed the changes in the gas-phase variables, for the typical time step used, cause only small effects on the solid-phase processes. On the other hand, the limited number of gas-phase solutions is a good compromise between the necessity of reducing the computational time and avoiding drastic variations in the predicted gas-phase variables. Constant conditions are assumed for the gas-phase during the time interval between two subsequent simulations.

2.3. Physical Properties and Kinetic Constants. Input parameters for the gas-phase equations (CFX model) and for the solid-phase model are listed in Tables 2 and 3, respectively. To take into account the formation of cracks and fissures in the char layer, the external surface, S_c, is increased by a factor of 8[3] in the evaluation of the gasification and combustion rates. The convective heat transfer coefficient, h_c, for the gasification/combustion of a single wood log is obtained from a correlation for cylindrical particles orthogonally heated by a gaseous flow.[33] The correlation is also used for the mass transfer coefficients, $h_{d,j}$.[17] Both heat and mass transfer coefficients are corrected to take into account transpiration effects.[34] Furthermore, a corrective factor has been determined for the global heat and mass transfer coefficients to take into account the effects of unsteadiness in reacting systems,[5] and the pre-exponential factors for the heterogeneous gasification

Table 3. Property Values and Kinetic Data for Poplar Wood Pyrolysis and Gasification

parameter	value	ref
A_{a1}	6.51×10^3 m/s	estimated
A_{a2}	4.45×10^4 m/s	estimated
A_p	4.37×10^6 m/s	19
c_l	4200 J/ kg K	20
c_c	1750 J/ kg K	17
c_u	2100 J/ kg K	20
c_v	1500 J/ kg K	20
c_w	1500 J/ kg K	19
E_{a1}	217 kJ/mol	35
E_{a2}	217 kJ/mol	35
E_p	143 kJ/mol	40
D	1.6×10^{-4} m²/s	1
k_c^*	0.42 W/ mK	19
k_w^*	0.3 W/ mK	19
n_{a1}	0.7	35
n_{a2}	0.5	24
x_{p,CH_4}	0.062	41, 42
$x_{p,CO}$	0.383	41, 42
$x_{p,CO2}$	0.237	41, 42
x_{p,H_2}	0.006	41, 42
x_{p,H_2O}	0.312	41, 42
x_{p,O_2}	0.0	41, 42
Δh_{a1}	1.44×10^4 kJ/kg	33
Δh_{a2}	1.1×10^4 kJ/kg	33
Δh_{a3}	-9.22×10^3 kJ/kg	33
Δh_p	430 kJ/kg	19
ν_v	0.8	19
ρ_w	460 kg/m³	1

reactions have been modified for the shrinking model applied here. The procedure employed for the evaluation of these parameters is briefly discussed below.

The corrective factor for the heat and mass transfer coefficients is determined using the experimental data by Dasappa et al.[12] for the combustion of single char particles. To describe the process, a heat conduction equation (with a symmetry condition at the center of the particle and a flux conservation at the surface) is coupled with mass balance for gas species (CO, O2, and N2) and char at the external surface. The convective heat transfer coefficient is obtained from the Ranz−Marshall equation,[35] which is also used for the mass transfer coefficients, $h_{d,j}$. The integral method is again used for the solution. A corrective factor of 0.53 gives the best agreement between predicted and measured conversion times, t_{90}, which is defined as the time when 90% conversion is achieved.

As the kinetic constants of the heterogeneous gasification reactions (a1−a2) in a shrinking wood particle are not available, the kinetic constants by Groenveld and van Swaaij[36] for CO2 gasification and Barrio et al.[24] for H2O gasification are modified. More precisely, corrections for the pre-exponential factors are obtained from the experimental data by Standish and Tanjung[37] and Dasappa et al.[13] for the gasification in CO2 and H2O environments of wood char spheres exposed to convective heating in a temperature-controlled furnace. By extension of the previously described model to include the effects of the gasification reactions (a1−a2), the pre-exponential factors are estimated (values listed in Table 3) according to the best-fitting procedure of the mass-loss histories. Predictions and measurements are compared in Figures 3−5. Figures 3 and 4 refer to the conversion, X, of Indonesian

(30) Bakke, J. R.; Hjertager, B. H. *Int. J. Numer. Methods Eng.* **1987**, *24*, 129−140.

(31) Magnussen, B. F.; Hjertager, B. H. *Proceedings of the 16th Symposium (International) on Combustion*; The Combustion Institute: Pittsburgh, 1976; pp 719−729.

(32) Lockwood, F. C.; Shah, N. G. *Proceedings of the 18th Symposium (International) on Combustion*; The Combustion Institute: Pittsburgh, 1981; pp 1405−1414.

(33) Perry, R. H.; Green, D. *Perry's Chemical Engineers' Handbook*, 6th ed.; McGraw-Hill: New York, 1985.

(34) Sherwood, T. K.; Pigford, R. L.; Wilke, C. R. *Mass Transfer*; McGraw-Hill: New York, 1975.

(35) Ranz, W. E.; Marshall, W. R. *Chem. Eng. Prog.* **1952,** *48*, 141−146, 173−180.

(36) Groeneveld, M. J.; van Swaaij, W. P. M. *Chem. Eng. Sci.* **1980**, *35*, 307−313.

(37) Standish, N.; Tanjung, A. F. A. *Fuel* **1988**, *67*, 666−672.

(38) Biba, V.; Macak, J.; Klose, E.; Malecha, J. *Ind. Eng. Chem. Process Dev. Des.* **1978**, *17*, 92−98.

(39) Yoon, H.; Wei, J.; Denn, M. M. *AIChE J.* **1978**, *24*, 885−903.

(40) Di Blasi, C.; Branca, C. *Ind. Eng. Chem. Res.* **2001**, *40*, 5547−5556.

(41) Adams, T. N. *Combust. Flame* **1980**, *39*, 225−239.

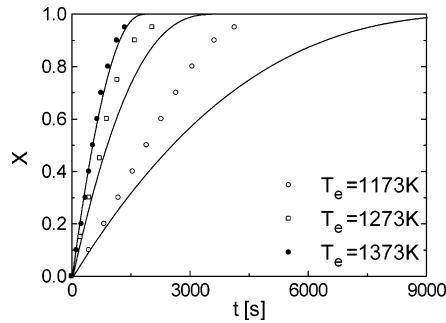(42) Boroson, M. L.; Howard, J. B.; Longwell, J. P.; Peters, A. W. *AIChE J.* **1989**, *35*, 120−28.

Figure 3. Predicted (lines) and measured (symbols) conversion, X, of Indonesian rubber tree charcoal vs time at different external temperatures, T_e.
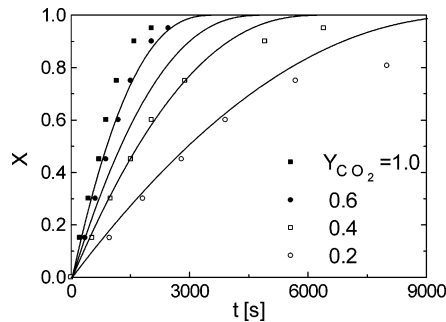

Figure 4. Predicted (lines) and measured (symbols) conversion, X, of Indonesian rubber tree charcoal vs time at different CO_2 external molar fractions, Y_{CO_2}.
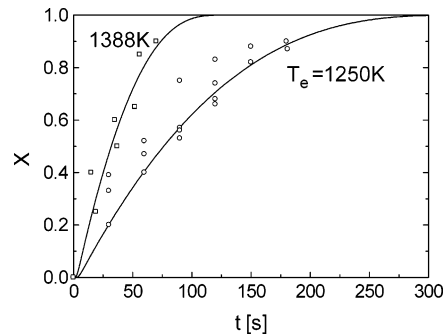

Figure 5. Predicted (lines) and measured (symbols) conversion, X, of ficus wood char vs time at different external temperatures, T_e.

Figure 6. Predicted (lines) and measured (symbols) conversion times, t_{90}, vs initial diameter, d_0, for different temperatures and compositions of the external gas phase.

Figure 7. Solid mass fraction, Y, mass-loss rate, $-dY/dt$, and the temperatures at the surface, T_s, pyrolysis front, T_p, and center, T_{ce}, of the solid as functions of time as predicted by the solid−gas-phase model for combustion conditions.

rubber tree charcoal versus time[37] in CO_2/N_2 environments for different CO_2 molar fractions and external temperatures, T_e (initial radius, R_0, of 0.011 m and char density, ρ_c, of 400 kg/m^3). The agreement between predictions and experiments is better at the highest temperatures and at the lowest CO_2 molar fractions, but after a sufficiently long time, the simulations always show a complete conversion. On the other hand, measurements show that, at low CO_2 molar fractions, complete conversion is not reached as a consequence of a possible reduction of active site density because of N_2 adsorption.[37] Figure 5 shows good agreement between the experimental and simulated results of the conversion, X, of Ficus wood char in a H_2O environment[13] for temperatures, T_e, of 1250 and 1388 K ($R_0 = 8$ mm, $\rho_c = 180$ kg/m^3).

To further check the validity of the modified gasification kinetics and to evaluate the effect of a diffusion-limited rate of the oxidation reaction, the measured[12] and the predicted conversion times, t_{90}, versus the initial diameter, d_0, are compared in Figure 6 ($\rho_c = 180$ kg/m^3). Experimental results cover the radius range of 0.0015−0.01 m, but the simulations are extended up to $R_0 = 0.02$ m. The results obtained in pure H_2O and pure CO_2 environments at $T_e = 1273$ K show that H_2O is far more reactive than CO_2. The predicted conversion times for CO_2 gasification are longer by factors 2.2 and 1.5 for radii of 0.002 and 0.02 m, respectively, compared to those obtained for H_2O gasification. In accordance with the assumed
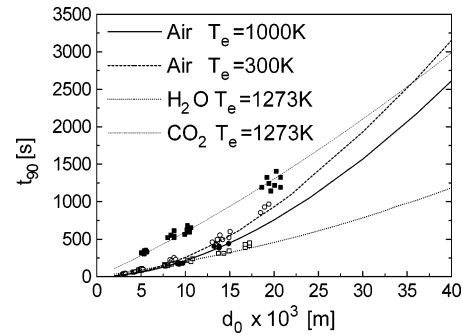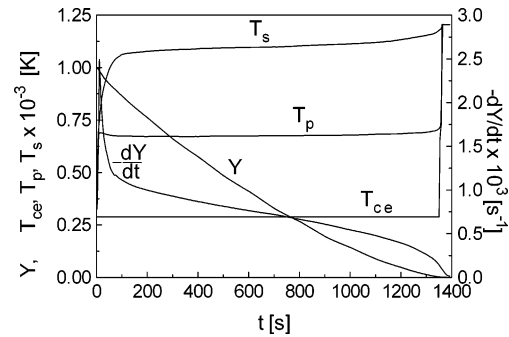
diffusion-limited reaction (a3), the dependence of the conversion times for combustion on the particle size, both at $T_e = 300$ and 1000 K, is stronger with respect to gasification. Thus, even if at low radii the combustion times are shorter than those of CO_2 gasification, at sufficiently large radii ($R_0 > 0.035$ m for combustion in air at $T_e = 300$ K) an inversion is observed. Moreover, since the oxidation reaction (a3) is assumed to be controlled by mass transfer, the conversion times present a d^2 law dependence. Thus, the differences between the conversion times predicted at low (300 K) and high (1000 K) external temperature (initial particle temperature equal to 900 K) are lower for smaller particles.

3. Results

Simulations have been made of the experimental tests presented by Bryden and Ragland[3] for poplar wood logs with an average length of 1.45 m (the main input and output variables are listed in Table 4). Tests N.3 and N.9 are discussed in detail as representative cases of combustion and gasification conditions. The simulations are made with the solid−gas-phase model and, for comparison purposes, with the solid-phase model.

3.1. Solid-Phase Dynamics. The main characteristics of the solid-phase dynamics, predicted by the coupled solid- and gas-phase model for the combustion test case can be seen from Figure 7 (solid mass fraction, mass-loss rate, and temperatures at the surface, the pyrolysis front, and the center of the sample as functions of time) and Figure 8 (position and propagation rate of the gasification/combustion, the pyrolysis, and the evaporation front as functions of time). The qualitative trends of the temperature profiles reproduce those already discussed[19,20] in the absence of char gasification/combustion. At the simulation start, the entire external heat flux is used for surface heating and moisture evaporation. Thus, mass loss begins soon, and an evaporation front appears (Figure 8). A maximum in the propagation rate of the pyrolysis front is also attained at short
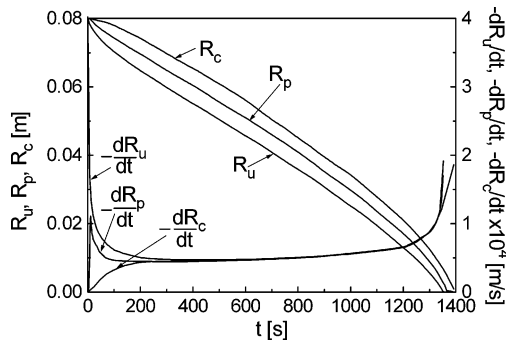
Figure 8. Positions R_u, R_p, R_c and propagation rates $-dR_u/dt$, $-dR_p/dt$, $-dR_c/dt$ of the evaporation, pyrolysis, and combustion/gasification fronts, respectively, as functions of time, as predicted by the solid−gas-phase model for combustion conditions.
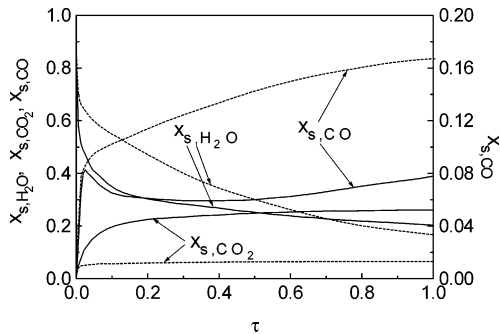

Figure 10. Heterogeneous gasification and combustion rates, ω_{O_2}, ω_{CO_2}, and ω_{H_2O}, as functions of nondimensional time, τ, as predicted by the solid−gas-phase model for combustion (solid line) and gasification (dashed line) conditions.

Figure 9. Species mass fractions, x_{s,CO_2}, x_{s,H_2O}, and $x_{s,CO}$, at the external surface of the wood log as functions of nondimensional time, τ, as predicted by the solid−gas-phase model for combustion (solid line) and gasification (dashed line) conditions.

times, and it essentially reproduces the exponential dependence on temperature.[19] The volatiles generated from wood decomposition add to steam and give rise to an increase in the mass loss rate, $-dY/dt$, followed by a maximum. However, because of internal heat transfer resistances, the propagation speeds of both the drying and pyrolysis fronts undergo significant reductions at relatively short times. In contrast, the propagation speed of the gasification/combustion front continuously increases with time, as a consequence of the increasing temperature at the external surface.

The large radius of the wood log and the severe thermal conditions in the external gas are responsible for the simultaneous occurrence of drying, pyrolysis, and char gasification/
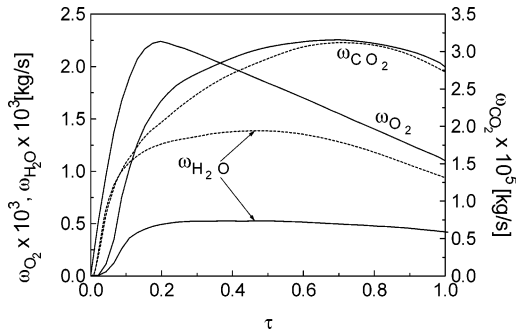
combustion. In other words, apart from the initial (about 200 s) and the final (about 1200 s) transients, the propagation speeds of the three fronts are roughly the same. Consequently, the thicknesses of dry wood and char also remain constant and are much smaller than the initial radius of the sample.

The main features of mass-loss dynamics for the gasification test case, where combustion reactions are absent, are not reported, because they are qualitatively similar to those in Figures 7 and 8. However, differences in the relevant variables at the solid/gas interface and surface reaction rates are not negligible. These can be seen from the profiles reported in Figure 9 (gas species mass fractions, x_{CO_2}, x_{H_2O}, and x_{CO}, at the external surface as functions of a nondimensional time, τ) and Figure 10 (gasification and combustion rates as functions of a nondimensional time, τ), respectively. The nondimensional time, τ, is the time normalized with the conversion times, t_{90}, which are very different for the combustion and for the gasification test (1080 and 1570 s, respectively).

The same qualitative trends are predicted in combustion and gasification for H_2O and CO_2 mass fractions. For both cases, the H_2O mass fraction decreases, whereas the CO_2 mass fraction increases, as a result of the decreasing ratio between the drying and the pyrolysis rates. As this ratio is higher for gasification until $\tau = 0.75$, the water mass fraction is also higher. The CO_2 mass fraction is about four times higher for combustion, probably as a consequence of higher concentration in the external gas-phase, because of the combustion reactions and larger CO_2 concentrations in the inlet flow. From the qualitative point of view, the trends of the CO mass fraction are different.

Table 4. Experimental Conditions, Measured Conversion Times, t_{90}, and Mean Mass-Loss Rates from 0 to 30%, v_1, from 30 to 60%, v_2, and from 60 to 90%, v_3, of Conversion for the Examined Tests[3]

|	input variables								output variables			
test	R_0 (m)	U_0	T_e (K)	u_e (m/s)	x_{e,O_2}	$x_{e,CO}$	x_{e,CO_2}	x_{e,H_2O}	t_{90} (s)	v_1 ($\times 10^3$ kg/s)	v_2 ($\times 10^3$ kg/s)	v_3 ($\times 10^3$ kg/s)
1	0.085	0.155	1253	0.7	0.024	0.0	0.139	0.109	3300	8	5	2.7
2	0.075	0.117	1363	0.7	0.088	0.0	0.141	0.110	1260	10	7	4.5
3	0.08	0.143	1423	0.8	0.18	0.0	0.127	0.099	1200	19	13	7.3
4	0.085	0.155	1353	0.77	0.197	0.003	0.121	0.098	1620	18	12	5.9
8	0.105	0.138	1613	0.6	0.0	0.084	0.055	0.146	2640	15	10	5.9
9	0.075	0.105	1613	0.6	0.0	0.084	0.055	0.146	1740	12	8	4.1
10	0.1	0.239	1563	0.58	0.233	0.0	0.0	0.006	1980	20	14	6.8
11	0.095	0.181	1573	0.58	0.233	0.0	0.0	0.006	1860	18	12	6.8
12	0.065	0.112	1333	0.82	0.18	0.0	0.127	0.099	1080	15	10	4.5
13	0.070	0.536	1313	0.7	0.029	0.001	0.134	0.106	2460	11	7	3.2
14	0.065	0.773	1363	0.7	0.107	0.001	0.138	0.108	1620	14	10	5.9
15	0.09	0.812	1253	0.7	0.181	0.002	0.124	0.10	2220	22	15	8.2
21	0.085	0.776	1553	0.58	0.232	0.0	0.0	0.006	2100	14	11	9.1
22	0.07	0.742	1563	0.54	0.0	0.0	0.154	0.121	1440	14	13	8.2
23	0.06	0.585	1393	0.68	0.014	0.084	0.069	0.014	1500	15	10	4.1
24	0.07	0.618	1603	0.98	0.18	0.0	0.127	0.099	1320	21	14	7.7
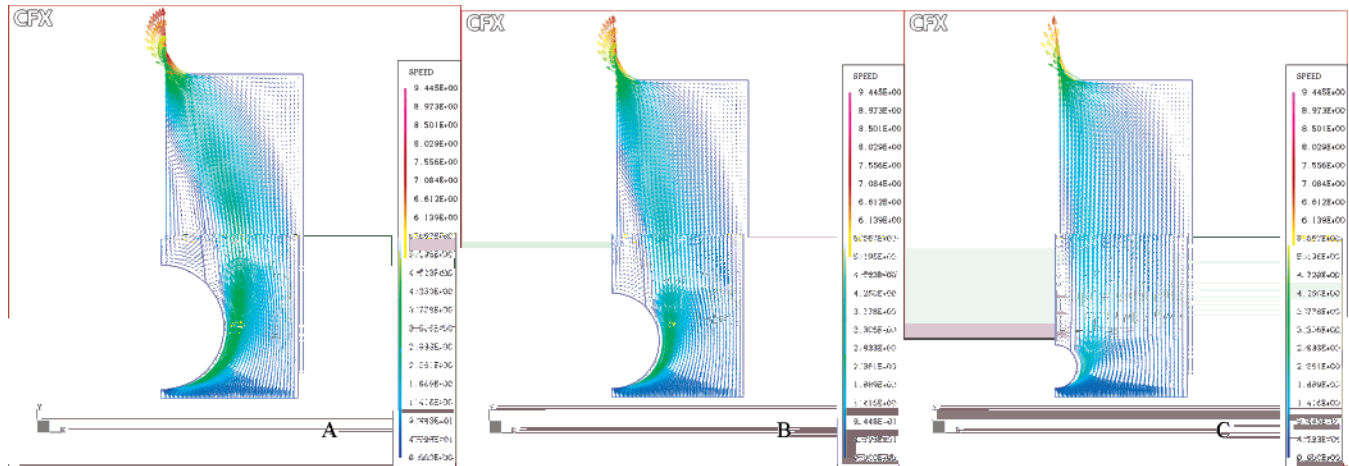
Figure 11. Vector velocity in the gas phase for conversion of 30 (A), 60 (B), and 90% (C) for combustion conditions.
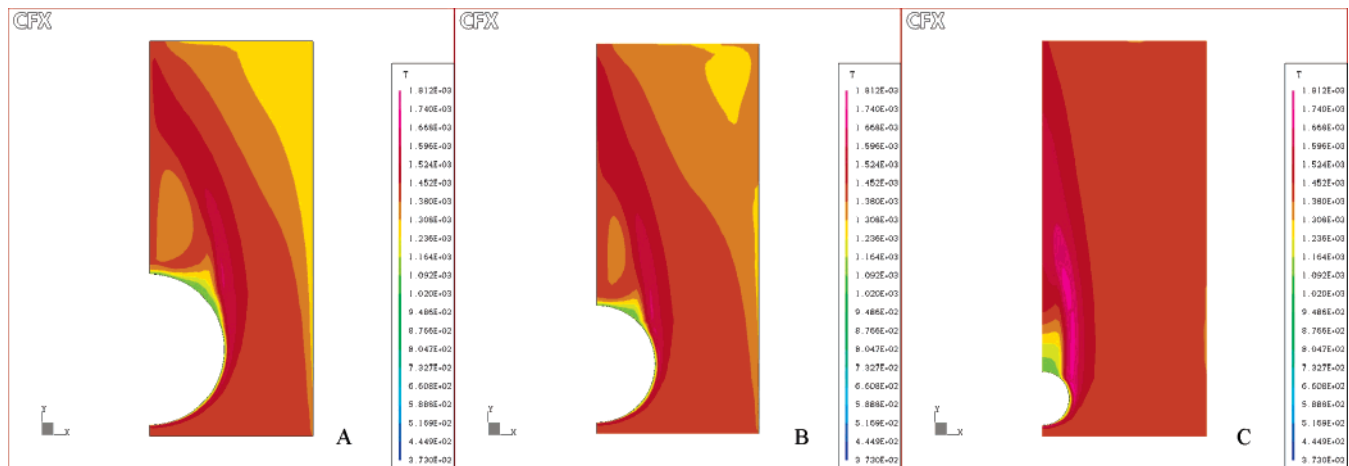

Figure 12. Color maps of temperature in the gas phase for conversion of 30 (A), 60 (B), and 90% (C) for combustion conditions.

In gasification, the CO mass fraction continuously increases with time, whereas in combustion the dynamics are more complicated, as a result of the consumption reactions in the gas phase. From a quantitative point of view, the CO mass fraction is roughly doubled for gasification. For both cases, H_2 and CH_4 mass fractions are much lower (not shown).

The reaction rates of char gasification by means of CO_2 and H_2O (Figure 9) are qualitatively similar along the considered time interval for both gasification and combustion. The two reaction rates increase with time, reach a maximum and then decrease. From the quantitative point of view, the CO_2 gasification rates are roughly coincident, whereas the H_2O gasification rate is higher for gasification by a factor of about 2.5, as a consequence of higher surface temperature (on average about 50 K) and H_2O mass fraction at the solid surface (Figure 9). The CO_2 gasification rates are much lower than the H_2O gasification rates by factors of about 20 and 50 for gasification and combustion, respectively. Similar to the gasification rates, the oxidation reaction rate increases, reaches a maximum, and then decreases. At short times, the high mass-loss rate from the solid prevents oxygen diffusion to the surface. Subsequently, the mass-loss rate decreases and the oxidation rate increases and reaches a maximum at $\tau = 0.2$. The following decrease depends above all on the reduction of the wood log external surface.

3.2. Gas-Phase Dynamics. An example of the gas-phase variables is given for the combustion test-case in terms of velocity vector fields (Figure 11A−C) and color maps of temperature (Figure 12A−C) and CO_2 mass fractions (Figure

13A−C) at 30, 60, and 90% of conversion (t_{30}, t_{60}, and t_{90}). The structure of the flow field, the temperature, and species concentrations vary with the conversion degree, and they are strictly coupled. In particular, the gas temperature and chemical species concentrations are significantly different from the inlet conditions, and they are strongly affected, among others, by the mass addition generated from solid conversion.

Figure 11A−C shows that a recirculation zone is always predicted in the upper right side of the furnace. During the initial stages, when the mass loss rate of the wood is sufficiently high, the gas flow is very close to the furnace walls (Figure 11A). When the radius of the sample is reduced, the gas trajectories are modified and become closer to its external surface (Figure 11C). A recirculation zone is also predicted in the center of the furnace above the solid for times shorter than $t = 1150$ s, when it disappears because of the reduced size of the wood sample and mass-loss rates. A maximum gas velocity of about 9.4 m/s is reached on the outlet surface, compared to values of 0.8 m/s for the velocity of the incoming gas flow and 0.18 m/s for the gas flow generated from wood conversion. Results are also qualitatively similar for gasification. In combustion, because of the exothermic reactions, the maximum temperatures exceed those assigned at the furnace inlet (by about 400 K). However, the temperatures of the gas layer adjacent the solid surface are always significantly lower (about 300 K) than the inlet values (Figure 12A−C). In contrast, during gasification, the temperatures in the chamber never exceed those assigned at the furnace inlet, and minimum values are attained in the gas layer adjacent to the solid surface with mean deviations of about 500 K from
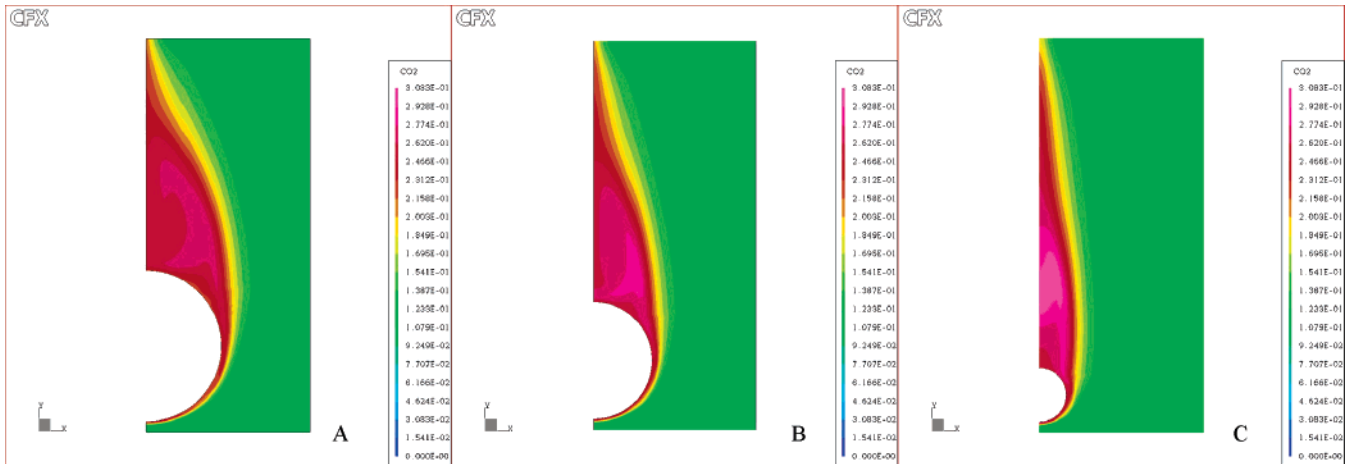
Figure 13. Color maps of CO_2 mass fractions in the gas phase for conversion of 30 (A), 60 (B), and 90% (C) for combustion conditions.
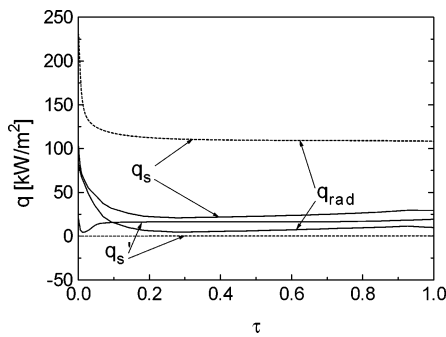

Figure 14. Global, q'_s, radiative, q_{rad}, and net, q_s, heat fluxes at the external surface of the wood log as functions of nondimensional time, τ, as predicted by the solid−gas-phase model (solid line) and by the solid-phase model (dashed line) for combustion conditions.

Figure 15. Species gas fluxes, F_{O_2}, F_{CO_2}, and F_{H_2O}, at the external surface of the wood log as functions of nondimensional time, τ, as predicted by the solid−gas-phase model (solid line) and by the solid-phase model (dashed line) for combustion conditions.

the inlet values. During combustion, the maximum O_2 mass fraction is constant and coincides with the inlet conditions at the furnace inlet. The concentration increases with increasing distance from the solid surface, where a zero value is assumed because of the infinitely fast reaction rate of the char oxidation reaction. Because CO_2 is a product of both wood pyrolysis and the gas-phase reactions, the maximum concentrations are not attained in the region adjacent to the solid but in the zone where CO and CH_4 mix and react with O_2. The maximum CO_2 mass fraction increases continuously with time as long as solid burning is under way (Figure 13A−C). During gasification, the maximum CO_2 mass fraction is much lower because of the lower inlet concentration and the absence of combustion reactions a4−a6. The maximum CO mass fraction is attained at the solid surface, and it increases with time. Furthermore, the CO mass fraction decreases with increasing distance from the solid surface, more rapidly for combustion than for gasification, in accordance with the reaction conditions. The concentrations of H_2 and CH_4 present a distribution qualitatively similar to that of CO.

3.3. Effects of a Simplified Gas-Phase Description. The differences between the main characteristics of the solid-phase dynamics, predicted by the solid−gas-phase model and the solid-phase model, mainly depend on the solid surface heat and mass fluxes. Therefore, only these variables are compared in Figures 14 and 15, using the combustion test as an example.

The heat fluxes, q'_s (see Nomenclature section), predicted by the two models, are qualitatively similar. A minimum value is observed to correspond with the maximum pyrolysis rate; then both fluxes increase. However, the solid-phase model predicts a flux that is lower on average by a factor of about 70. The
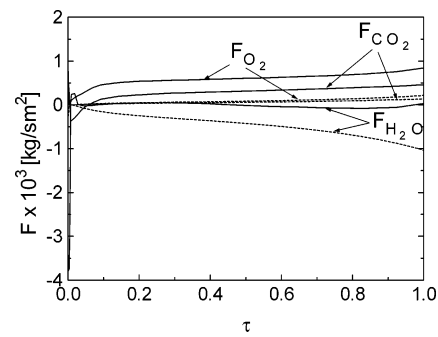
radiative heat flux, q_{rad}, predicted by the solid-phase model, decreases continuously with τ, because of the reduction of the difference between the external and surface temperature. The radiative flux predicted by the solid−gas-phase model decreases for $\tau < 0.28$, as a result of the increase in the surface temperature and the decrease in the mean gas-phase temperature (because of the mixing between the hot inlet gas and the colder gases coming from the degrading solid phase). When the exothermic gas-phase combustion reactions become active, the radiative flux increases until $\tau < 0.93$. Then, the mean gas-phase temperature decreases, and a new decrease in radiative flux is again observed. The predictions of the two models are quantitatively very different. The net heat flux to the solid surface, calculated as the sum of q_{rad} and q'_s, predicted by the solid-phase model, has an average value of 110 kW/m² which is about four times higher than that calculated by the solid−gas-phase model (Figure 14).

Figure 15 shows that the O_2 and CO_2 mass fluxes to the solid surface predicted by the solid−gas-phase model and by the solid-phase model increase with time (except for the short time interval $\tau < 0.01$). For the solid-phase model, this trend is the result of increasing values of the mass transfer coefficient and the difference of the CO_2 mass fraction between environment and the surface. On the other hand, for the solid−gas-phase model, this result depends on the increasing gradients of the gaseous species at the surface. The solid−gas-phase model predicts an average oxygen mass flux of 6.6×10^{-4} kg/s m, which is about 3.2 times higher than the solid-phase model. This result depends on the underestimation of the mass transfer coefficient. Namely, in the solid-phase model it is assumed that the O_2 mass fraction of the gas phase coincides with the inlet (maximum) value. Because of the small mass transfer coef-
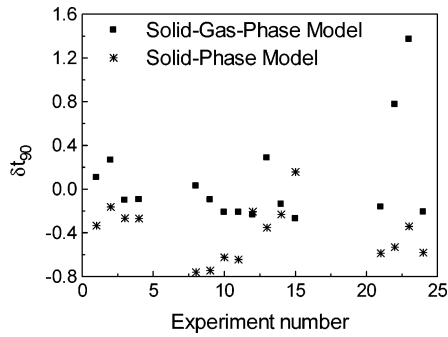
Figure 16. Deviations of the conversion times, t_{90}, predicted by the solid−gas-phase model and the solid-phase model, with respect to measurements.[3]
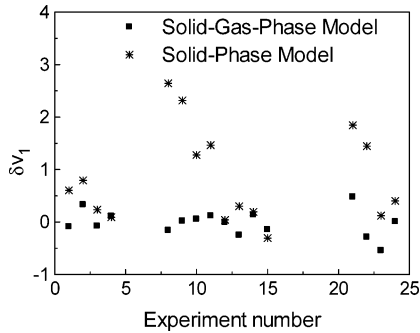

Figure 17. Deviations of the mean mass-loss rates from 0 to 30%, v_1, of conversion, predicted by the solid−gas-phase model and the solid-phase model, with respect to measurements.[3]

Figure 18. Deviations of the mean mass-loss rates from 30 to 60%, v_2, of conversion, predicted by the solid−gas-phase model and the solid-phase model, with respect to measurements.[3]

Figure 19. Deviations of the mean mass-loss rates from 60 to 90%, v_3, of conversion, predicted by the solid−gas-phase model and the solid-phase model, with respect to measurements.[3]

ficients and the limited differences between the CO_2 mass fractions in the furnace and at the solid surface, the CO_2 mass flux predicted by the solid-phase model is lower than that predicted by the comprehensive model by a factor of about 3. The H_2O mass flux predicted by the solid-phase model alone and by the solid−gas-phase model are qualitatively and quantitatively different. An almost constant flux of -1.3×10^{-5} kg/m^2 s is predicted by the solid−gas-phase model. The flux predicted by the solid-phase model is always negative and decreases with τ. This result indicates that the effect of the increasing mass transfer coefficient,[34] resulting from the reduction of the mass efflux from the solid phase, is larger than the effect of the decreasing difference between the H_2O mass fractions in the gas phase and at the solid surface.

The conversion times, t_{90}, predicted by the solid−gas-phase model and by the solid-phase model are 1080 and 882 s, respectively. They are very close to each other compared to the large differences in the heat fluxes and the gaseous species mass fluxes. This is the result of compensation effects between the higher external heat flux and the lower O_2 flux predicted by the solid-phase model.

3.4. Experimental Validation. The predictions of both the solid−gas-phase and solid-phase models are compared to the measurements by Bryden and Ragland,[3] in terms of deviations of the conversion times, t_{90}, (Figure 16) and of the mean mass-loss rates from 0 to 30%, v_1, from 30 to 60%, v_2, and from 60 to 90%, v_3, of conversion (Figures 17−19) with respect to experimental values. The predictions of the solid−gas-phase model are more accurate than those of the solid-phase model, which underestimates the conversion time and, consequently, overestimates the mean mass-loss rates for most cases. The mean deviation of the conversion time, in absolute value, predicted by the solid−gas-phase and the solid-phase model are 29 and 42%, respectively. The mean deviations of the mean mass-loss rates v_1, v_2, and v_3 are 18, 18, and 40%, respectively, when
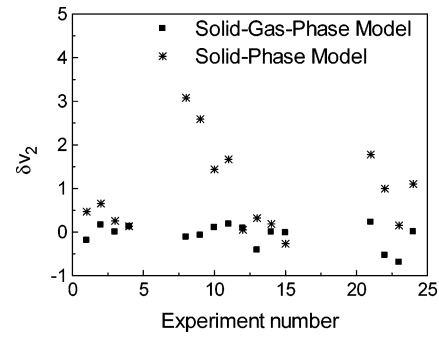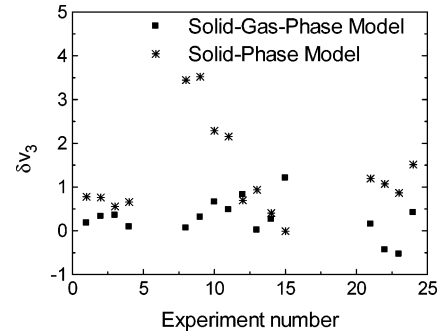
using the solid−gas-phase model, and 88, 95, and 130%, respectively, when using the solid-phase model.

It is worth noting that, as pointed out by Galgano and Di Blasi,[17] the results are not affected by buoyancy effects, which are neglected in the solid-phase model. In this way, the differences between the conversion times obtained with the two models are caused, above all, by the reduction of the gas temperature following wood drying and decomposition and the higher oxidation rates predicted by the solid−gas-phase model. Since these effects compensate for each other in the prediction of the conversion times, the largest differences are observed in gasification, where the char oxidation reaction is absent. These results indicate that, to get quantitative predictions of wood combustion/gasification, a coupling is needed between comprehensive descriptions of both the solid- and the gas-phase processes. Nevertheless, the predictions of the solid-phase model could be improved through the formulation of simplified models for the description of the gas-phase thermal field and the introduction of corrective factors for heat and mass transfer coefficients or the use of correlations specifically developed for the problem of interest.

4. Conclusions

A comprehensive model for the gasification and combustion of thick wood particles, coupled with a CFD model for the gas-phase processes previously developed, has been extensively studied, after a re-examination of the kinetic constants for the heterogeneous gasification reactions for a shrinking char particle. Simulations of combustion and gasification are compared. Mass-loss dynamics are qualitatively similar, except for the surface concentration of CO, which in the former case is involved in the combustion process.

Detailed simulations of the gas-phase processes show that the structure of the flow field strongly interacts with the

temperature and the chemical species distribution. The solid- and gas-phase processes are strictly coupled and affect each other, as a result of the mass outflow from the solid surface and the activity of homogeneous reactions.

The results obtained with the solid−gas-phase model are compared to those given by the solid-phase model, where the gas-phase processes are approximated by global heat and mass transfer coefficients and constant values of the external variables. Again, the mass-loss dynamics are for a large part qualitatively similar for both models. When the solid-phase model alone is considered, a critical issue is the selection of appropriate correlations for the global heat and mass transfer coefficients. For the cylindrical geometry considered here, results show that the total heat flux is overestimated and the char combustion rate is underestimated.

The solid−gas-phase model is validated by comparison between the predicted and the experimental conversion times and mean mass-loss rates for widely variable experimental conditions. The agreement is acceptable, with mean deviations, in absolute value, of 29% for the conversion time and 18, 18, and 40% for the mean mass loss rates from 0 to 30%, v_1, from 30 to 60%, v_2, and from 60 to 90%, v_3, respectively, of conversion. Higher deviations are predicted by the solid-phase model, which generally underestimates the conversion times and overestimates the mean mass-loss rates. The introduction of a corrective factor for the heat and mass transfer coefficient could allow improvements in the predictions of the solid-phase model.

Nomenclature

A = preexponential factor
C = gas species concentration (kmol/m^3)
c = specific heat (J/kg K)
D = diffusion coefficient (m^2/s)
e = surface emissivity
E = activation energy (kJ/mol)
F = diffusive mass flux (kg/m^2 s)
k = turbulent kinetic energy (m^2/s^2)
k_g = gas thermal conductivity (W/m K)
k^* = thermal conductivity (W/m K)
h_c = convective heat transfer coefficient (W/m^2 K)
h_d = global mass transfer coefficient (kg/m^2 s)
L = length (m)
M = molecular weight (kg/kmol)
m_p = mass flux of volatile pyrolysis products (kg/s)
m_u = water vapor mass flux (kg/s)
m_v = volatile mass flux per unit surface (kg/m^2 s)
n = reaction order
q = heat flux (W/m^2)
$q_s = q'_s + q_{rad}$ = net heat flux (W/m^2)
q_s = global heat flux (W/m^2)
q_{rad} = radiative heat flux (W/m^2)
r = radial coordinate
$\mathcal{R}$ = universal gas constant (kJ/mol K)
R = particle radius (m)
Re = Reynolds number
s = stoichiometric coefficient
S = surface (m^2)
t = time (s)
T = temperature (K)
U_0 = moisture content
v = mean mass loss rate (g/min)
x = mass fraction
y = mole fraction

Y = total solid-phase mass fraction (%)
b = absorption coefficient of the gas phase (m^{-1})
Δh = reaction enthalpy (J/kg)
δ = deviation of the predictions with respect to the the experiments
ϵ = dissipation of turbulent kinetic energy (m^2/s^3)
$\tilde{\lambda}$ = enthalpy of water evaporation (J/kg)
v_v = volatile fraction
ρ = density (kg/m^3)
ω = gas-phase reaction rate (kg/m^3 s)
$\bar{\omega}$ = heterogeneous reaction rate (kg/s)
ω_p = pyrolysis rate (kg/s)

Subscripts

a1 = carbon dioxide gasification
a2 = steam gasification
a3 = char oxidation
a4 = carbon monoxide combustion
a5 = hydrogen combustion
a6 = methan combustion
a7 = water−gas shift
b = boiling point
C = char
ce = particle center
CH_4 = methane
CO = carbon monoxide
CO_2 = carbon dioxide
e = external
E = equilibrium
g = gas phase
H_2 = hydrogen
H_2O = steam
i = chemical reaction
j = gas-phase chemical species
k = kinetic
l = liquid water
O_2 = oxygen
p = pyrolysis front
s = external surface
u = drying front
v = volatiles
w = dry virgin wood
0 = initial
30 = total conversion equal to 30%
60 = total conversion equal to 60%
90 = total conversion equal to 90%